Sound & Vibration 2025, 59(2), 2952.
https://doi.org/10.59400/sv2952

Article

The relationship between installation stiffness and the natural characteristics of reinforced cylindrical shells and its application to structural vibration mitigation design

Lufei Li[1], Jincheng Gao[2], Jingyi Xiong[2], Fuzhen Pang[1], Cong Gao[1], Haichao Li[1,*]

[1] College of Shipbuilding Engineering, Harbin Engineering University, Harbin 150001, China
[2] Wuhan Second Ship Design and Research Institute, Wuhan 430061, China
*** Corresponding author:** Haichao Li, lihaichao@hrbeu.edu.cn

CITATION

Li L, Gao J, Xiong J, et al. The relationship between installation stiffness and the natural characteristics of reinforced cylindrical shells and its application to structural vibration mitigation design. Sound & Vibration. 2025; 59(2): 2952. https://doi.org/10.59400/sv2952

ARTICLE INFO

Received: 17 March 2025
Accepted: 25 April 2025
Available online: 6 May 2025

Abstract: The study primarily focuses on the impact of the installation stiffness at the bottom of the reinforced cylindrical shell on its natural characteristics. Using the finite element modal analysis method, it systematically investigates the effects of three installation stiffness forms—rigid base, rubber pad-supported base and isolator-supported base on the natural frequencies and mode shapes of the stiffened cylindrical shell. Additionally, the influence of key parameters such as rubber pad thickness and elastic modulus on the natural characteristics of the stiffened cylindrical shell is examined. The results show that as installation stiffness increases, the natural frequencies of the stiffened cylindrical shell significantly rise, with a more pronounced effect on lower-order modes. The rubber pad-supported base maintains vibration characteristics close to those of the free state, particularly above 50 Hz. Furthermore, increasing the rubber pad thickness and decreasing the elastic modulus both lead to a reduction in natural frequency, particularly for lower-order modes, which are more sensitive to these parameter changes. These findings provide important guidance for optimizing the vibration characteristics and isolation design of stiffened cylindrical shell structures.

Keywords: near-free vibration isolation design; stiffened cylindrical shell; finite element analysis; installation stiffness; natural frequency

1. Introduction

The stiffened cylindrical shell structure, with its central symmetry and excellent mechanical properties, is widely used in key fields such as aerospace, mechanical engineering, and naval architecture [1–3]. It is particularly applied in scenarios such as pressure-resistant hulls of underwater vehicles, weapon launch tubes, and aircraft fuselages [4–6]. The vibration characteristics of cylindrical shells determine the structural noise radiation, fatigue life, and operational stability. However, in practical engineering applications, shells are often connected to external structures through bases, vibration isolators, and other support systems, where variations in installation stiffness can significantly alter boundary conditions, thereby affecting natural frequencies and mode shapes. Improper design may lead to increased resonance risk and higher vibration transmission efficiency. Therefore, investigating the influence of installation stiffness on the natural characteristics of cylindrical shells is of great engineering significance for optimizing vibration isolation design, preventing resonance damage, and enhancing equipment reliability [7].

In recent years, significant progress has been made in the study of shell structure vibration characteristics and stiffness effects. Liu et al. [8] proposed a magnetic

higher-order stable quasi-zero-stiffness (QZS) mechanism, and analyzed its frequency response characteristics without involving polynomial approximation. Li et al. [9] introduced a unified Jacobi-Ritz-spectral boundary element method (BEM) for spherical shells, which offers high-precision solutions for complex boundary conditions. Liu et al. [10] systematically examined research advancements in quasi-zero stiffness vibration isolation technology from the perspectives of design optimization, improvement strategies, and engineering applications. This innovative approach enables significant reduction of dynamic stiffness while maintaining static stiffness integrity, thereby effectively extending the vibration isolation frequency band into the low-frequency domain. Liu et al. [11] developed a novel quasi-zero stiffness configuration integrating four piezoelectric buckling beams with vertical spring elements. This device leverages negative stiffness characteristics to achieve dual functionality: lowering the fundamental vibration isolation frequency while simultaneously enhancing electrical energy output through piezoelectric conversion. Xu et al. [12] analyzed the effect of transmission stiffness on the open-loop transfer function of the rudder servo system, finding that increasing transmission stiffness raises the anti-resonant and resonant frequencies of the rudder servo system. Wang et al. [13] studied the free vibration characteristics of shells under arbitrary boundary conditions and solved the dynamic differential equations of shells with arbitrary boundary conditions. Emad et al. [14] solved the problem to illustrate the effects of the changes in geometry, material, and elastic boundary conditions (EBCs) on the natural frequency fluctuations (NFFs) of the ASCCS structure. Li [15] investigated the influence of orthotropic properties and boundary conditions on the free vibration of rotating, truncated, circular orthotropic conical shells. Pang et al. [16] According to different scenarios applicable to paraboloidal shell structures, artificial spring techniques are employed to simulate complex boundary conditions including free, simply supported, and fully clamped edges. This approach is used to verify the convergence of the Jacobi-Ritz spectral boundary element method. Li et al. [17] studied the impact of joint stiffness and joint size on the load-bearing capacity of single-layer cylindrical reticulated shells. Gao et al. [18] investigated the free and forced vibration characteristics of uniform and stepped coupled shell structures with arbitrary boundary conditions. Zheng et al. [19] proposed a unified and efficient method for analyzing the vibration characteristics of conical shells with arbitrarily varying thickness and elastic boundary conditions.

The aforementioned literature, through studies in various fields, has demonstrated that installation stiffness, support parameters, and material and geometric design have a significant impact on the natural frequencies, vibration characteristics, and transmission properties of structures [20,21]. Existing work has mostly focused on optimizing the support stiffness of electromechanical systems, shaft assemblies, or simple shells, and in most studies, spring models are used to represent boundary stiffness. However, the relationship between installation stiffness and the vibration characteristics of stiffened cylindrical shells, a typical structure has not been fully explored. Therefore, this study takes the stiffened cylindrical shell as the research object. Using the finite element method, it systematically compares for the first time the modal characteristics of the stiffened cylindrical shell under three different installation stiffness conditions, focusing on analyzing the effects of three installation

stiffness forms—rigid base, rubber pad-supported base, and isolator-supported base—on natural frequencies. By comparing the changes in natural frequencies under different installation stiffness conditions, the influence of installation stiffness on the inherent properties of the stiffened cylindrical shell is thoroughly investigated. Additionally, a quantitative sensitivity analysis of natural frequencies is conducted based on theoretical formulas. These findings not only provide a theoretical basis for vibration control and installation design of stiffened cylindrical shells but also offer practical guidance for optimizing parameter selection in vibration isolation support designs, demonstrating significant engineering application value.

2. Theoretical analysis

2.1. Dynamic equation of the cylindrical shell

The vibration system is usually a distributed-parameter system, and due to its continuity, directly solving for the natural frequencies and mode shapes is quite difficult. To simplify the analysis, it is typically discretized into a system with finite degrees of freedom, and the differential equations governing its free motion are established. The finite element dynamic equation for the cylindrical shell is expressed as follows [22]:

$$\mathrm{M}\ddot{u} + \mathrm{C}\dot{u} + \mathrm{K}u = 0 \tag{1}$$

In Equation (1), M represents the structural mass matrix, C denotes the structural damping matrix, K is the structural stiffness matrix, and u is the nodal displacement vector.

Modal analysis aims to obtain the natural frequencies and mode shapes of the system, which are primarily determined by the mass matrix and stiffness matrix. In engineering applications, structural damping is usually small and has a relatively limited effect on natural frequencies and mode shapes. The equation can be simplified as:

$$\mathrm{M}\ddot{u} + \mathrm{K}u = 0 \tag{2}$$

The two fundamental paradigms of vibration analysis reveal the intrinsic characteristics of a system. The Fourier transform decomposes any complex vibration signal into harmonic components in the frequency domain, while the modal superposition principle decouples the structure's free vibration into a linear combination of its natural modes. The exponential function $e^{j\omega t}$ naturally represents the combination of sine and cosine functions: $e^{j\omega t} = \cos(\omega t) + j\sin(\omega t)$, Thus, the free vibration solution is assumed to take the form:

$$u(t) = \phi e^{j\omega t} \tag{3a}$$

$$\dot{u}(t) = j\omega\phi e^{j\omega t} \tag{3b}$$

$$\ddot{u}(t) = -\omega^2\phi e^{j\omega t} \tag{3c}$$

where ω represents the natural frequency of the cylindrical shell, and ϕ is the eigenvector describing the vibration mode shape in this modal state.

Substituting the above expression into the dynamic equation:

$$\mathrm{M}\left(-\omega^2\phi e^{j\omega t}\right)+\mathrm{K}\phi e^{j\omega t}=0 \tag{4}$$

After simplification, the eigenvalue problem can be obtained as:

$$\left((-\omega^2)\mathrm{M}+\mathrm{K}\right)\phi=0 \tag{5}$$

Solving Eigenvalues: Since the mass matrix M and stiffness matrix K are often large-scale sparse matrices, the Lanczos method is employed for solving them. The Lanczos method is an efficient iterative algorithm for computing eigenvalues of large sparse symmetric matrices by transforming the symmetric matrix into a symmetric tridiagonal matrix through orthogonal similarity transformations [23]. The core idea of this method lies in projecting the eigenvalue problem onto a low-dimensional Krylov subspace spanned by a set of orthogonal vectors. A Krylov subspace is a linear subspace formed by the initial vector v and the vectors generated by repeatedly applying matrix A, expressed as follows [24]:

$$\kappa_m(A,v)=span\{v,Av,A^2v,\dots,A^{m-1}v\} \tag{6}$$

where κ_m denotes the constructed Krylov subspace, A is the object matrix for constructing the subspace, and v is the initial vector.

By constructing a tridiagonal matrix within this subspace that effectively approximates the original system, the Lanczos method can efficiently compute the first few natural frequencies and mode shapes of the structural system in a reduced-dimensional space.

2.2. Incorporation of mounting stiffness

The total stiffness matrix of the structure is obtained by adding a support stiffness matrix $\mathbf{K_{support}}$ to the overall finite element stiffness matrix **K**, where the support stiffness matrix has non-zero entries only in the rows and columns corresponding to the support nodes. The total stiffness matrix is given by:

$$\mathrm{K_{total}}=\mathrm{K}+\mathrm{K_{support}} \tag{7}$$

The dynamic equation of the structure is expressed as:

$$\mathrm{M}\ddot{u}+\mathrm{K_{total}}u=0 \tag{8}$$

The eigenvalue equation with supports can be obtained as:

$$\left((-\omega^2)\mathrm{M}+\mathrm{K_{total}}\right)\phi=0 \tag{9}$$

The natural frequency ω_i is determined by the eigenvalues of the stiffness matrix $\mathrm{K_{total}}$ and the mass matrix M, and satisfies:

$$\omega_i=\sqrt{\frac{k_i}{m_i}} \tag{10}$$

where k_i and m_i are the i-th generalized eigenvalues of the stiffness matrix and the mass matrix, respectively.

2.3. The sensitivity of the natural frequency to the installation stiffness

Starting from the eigenvalue equation, consider differentiating with respect to k_j. Expanding, we obtain:

$$2\omega_i \frac{\partial \omega_i}{\partial k_j} M\phi_i + \omega_i^2 M \frac{\partial \phi_i}{\partial k_j} = \frac{\partial K_{total}}{\partial k_j}\phi_i + K_{total}\frac{\partial \phi_i}{\partial k_j} \tag{11}$$

Multiplying both sides of the equation by ${\phi_i}^T$ on the left, the above equation can be simplified as:

$$\frac{\partial \omega_i}{\partial k_j} = \frac{1}{2\omega_i}{\phi_i}^T \frac{\partial K_{total}}{\partial k_j}\phi_i \tag{12}$$

Since in this partial derivative matrix, only the degree of freedom corresponding to the applied stiffness k_j has a value of 1, and all other positions are 0, Equation (11) can be further simplified as:

$$\frac{\partial \omega_i}{\partial k_j} = \frac{1}{2\omega_i}\left(\phi_{i,j}\right)^2 \tag{13}$$

where $\left(\phi_{i,j}\right)$ represents the component of the i-th mode at the j-th installation degree of freedom.

The impact of installation stiffness on the natural frequency of the cylindrical shell can be further expressed as:

$$\Delta\omega_i \propto \sum_j \frac{\left(\phi_{i,j}\right)^2}{2\omega_i}\Delta k_j \tag{14}$$

where $\Delta\omega_i$ is the change in the system's natural frequency ω_i due to the variation in the installation stiffness k_j and Δk_j is the change in the installation stiffness at position j.

3. Model description

3.1. Stiffened cylindrical shell geometric model

This study focuses on the stiffened cylindrical shell structure, with one end open and the other closed. The structure consists of the cylindrical shell body, internal raft base, and internal ring ribs that enhance the structural strength. The three-dimensional model of the stiffened cylindrical shell structure was established in CATIA software, as shown in **Figure 1**. The model has a total length of L = 3500 mm, a radius of R = 1500 mm, a shell thickness h = 6 mm, and rib spacing of 700 mm. The circumferential reinforcement ribs are flat steel with dimensions of 10 mm × 90 mm. All components of the structure are made of steel material, with a density of ρ = 7850 kg/m^3, Young's modulus $E = 2.1 \times 10^{11}$ Pa, and Poisson's ratio μ = 0.3. The total weight of the structure is 2876.06 kg.

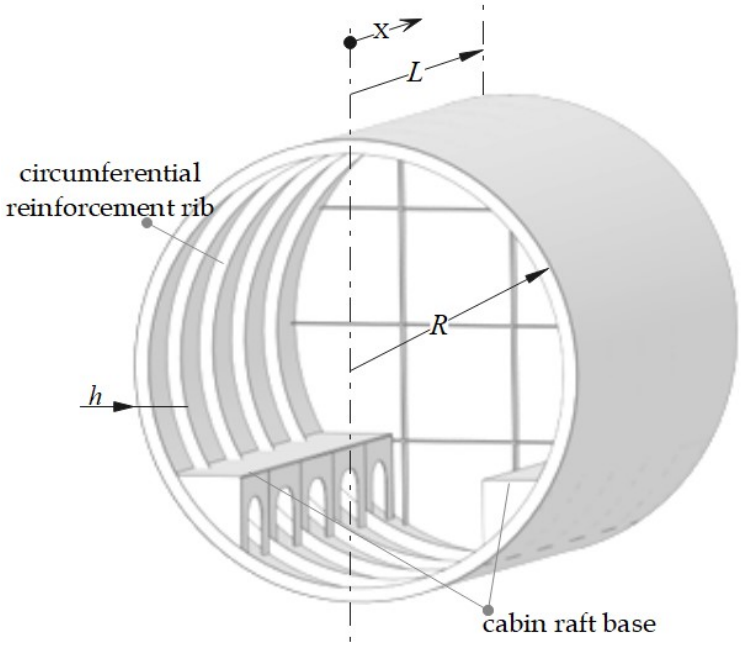

Figure 1. Stiffened cylindrical shell geometrical model.

3.2. Installation base geometrical model

According to the research objectives, finite element models for three typical support forms—rigid base, rubber pad-supported base, and vibration isolator-supported base—have been established. The design features and parameter settings are as follows:

Rigid base: As displayed in **Figure 2**, the base is rigidly fixed to the ground, and the shell is directly placed on the base without any flexible connection. This results in an increase in the overall system stiffness. The dimensions of the base are L' = 3000 mm, B = 1800 mm, and H = 400 mm.

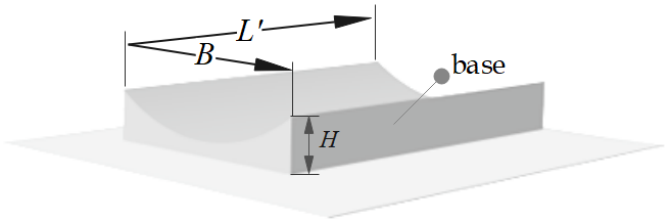

Figure 2. Schematic of rigid base.

Rubber pad support base: In this study, neoprene rubber was selected as the material for the rubber pad, with the following parameter settings based on the supplier's data: The density range is 1230–1300 kg/m^3, and the Young's modulus is between 2–5 MPa. Additionally, the common thickness range for rubber pads in the market is 10–100 mm. Based on this data, a rubber layer with a thickness of 50 mm was added between the shell and the base, as shown in **Figure 3**. In Abaqus, the rubber layer was defined as a linear elastic material with a density of 1230 kg/m^3, a Young's modulus of 3 MPa, and a Poisson's ratio of 0.48.

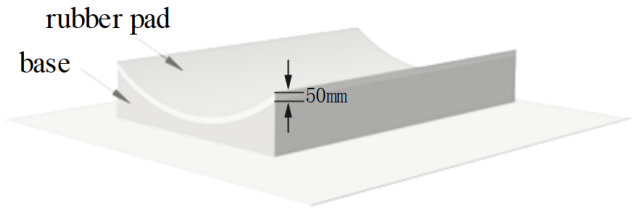

Figure 3. Schematic of the rubber pad support base.

Vibration isolator support base: The system utilizes 20 BE-220 vibration isolators (parameters listed in **Table 1**) to connect the shell and base. In accordance with engineering vibration isolation design standards [25], the isolators are symmetrically arranged at equal intervals along the base direction [26], as shown in **Figure 4**.

Table 1. Vibration isolator parameters.

Model	Rated static deformation	Installation condition		Dynamic stiffness (kN/m)		
		Number (pcs)	Arrangement	Y	X	Z
BE-220	3–5 mm	20	Two-row symmetrical arrangement	2268	816	880

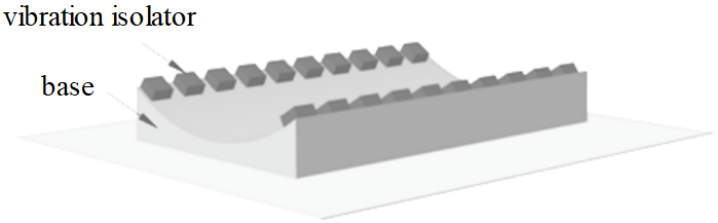

Figure 4. Schematic of the vibration isolator support base.

In Abaqus, the modeling of the vibration isolator-supported base uses spring elements to simulate the supporting effect of the vibration isolators [27]. The specific implementation method is as follows: First, connection points are defined at corresponding positions between the shell and the base, and spring elements are applied between these points to simulate the supporting characteristics of the vibration isolators. To accurately describe the directional stiffness characteristics of the vibration isolators, a local coordinate system is established to define the action direction of the vibration isolators. Based on this, spring elements are arranged along the three orthogonal directions (X, Y, Z) at each connection point, and the corresponding directional stiffness values are assigned, where the isolators on the left side are numbered 1–10 and those on the right side are numbered 11–20 (as shown in **Figure 5**).

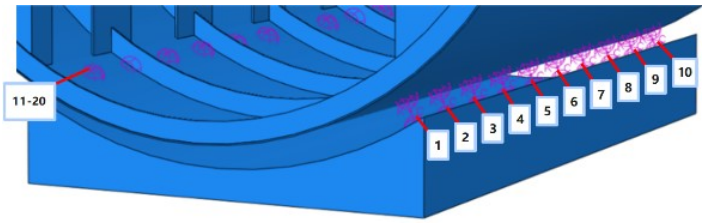

Figure 5. Schematic of the vibration isolator support base.

3.3. Mesh convergence analysis

To ensure the accuracy and reliability of the finite element analysis results, this study conducted a mesh convergence analysis on the computational model.

When performing the mesh division, the element type used was C3D8R. For the free-state model, a mesh size of 25 mm was used, resulting in a total of 94,609 elements. Under the rigid base, the base section consisted of 142,080 elements, with the overall model having a total of 236,689 elements. For the rubber pad-supported base, the base section consisted of 162,480 elements, with the overall model having a total of 257,089 elements. The isolator-supported base had 142,080 mesh elements, and the overall model consisted of 236,689 elements.

To ensure the accuracy of the results, a mesh convergence test was conducted. Following the empirical rule that "5–7 nodes should be included within one wavelength range" for vibration analysis, simulation results for different element sizes (25 mm, 20 mm, 15 mm) were compared. The rate of change in the natural frequency was used as the criterion for convergence. After further refining the mesh, the variation in the calculated natural frequency was less than 2%, indicating that the results had converged.

4. Structural modal analysis and results analysis

Based on the established model, the effect of installation stiffness on the free vibration characteristics of the stiffened cylindrical shell is discussed using the finite element software Abaqus [28]. The natural frequencies and mode shapes for each condition are obtained through modal analysis. Specifically, this includes four conditions: free state, rigid base, rubber pad-supported base, and vibration isolator-supported base.

4.1. Modal analysis under the free state

Figure 6 shows the finite element model of the structure under free state conditions, where no constraints are applied. This model serves as the baseline for understanding the natural vibration characteristics of the system.

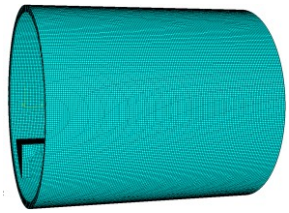

Figure 6. Finite element model of the structure in the free state.

The first six natural frequencies of the structure in this state are shown in **Table 2**, and the corresponding mode shape cloud diagrams are shown in **Figure 7**.

Table 2. Natural frequency in the free state.

Mode order	1 (Hz)	2 (Hz)	3 (Hz)	4 (Hz)	5 (Hz)	6 (Hz)
Free state	22.1	26.8	62.8	66.5	115.4	124.9

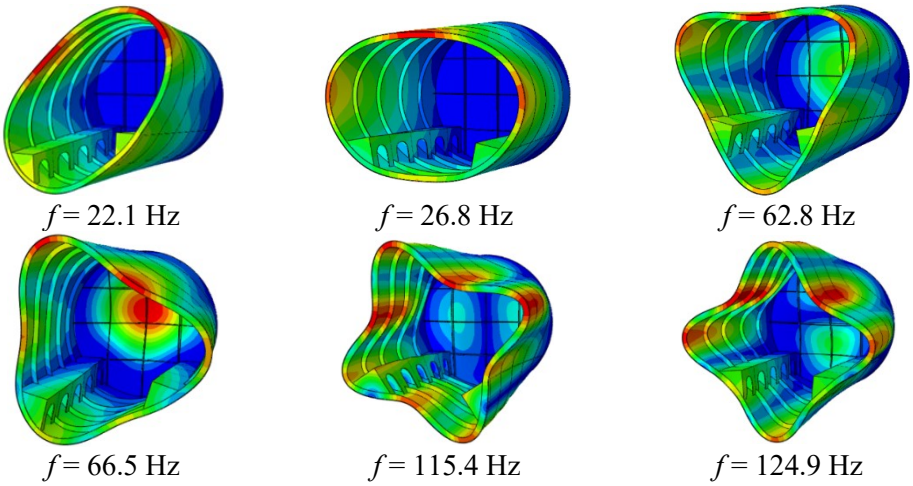

Figure 7. Mode shape cloud diagram in the free state of the structure.

4.2. Modal analysis under a rigid base

The finite element model of the structure supported by a rigid base is shown in **Figure 8**. This model is used to simulate the vibration characteristics of the structure under rigid installation conditions.

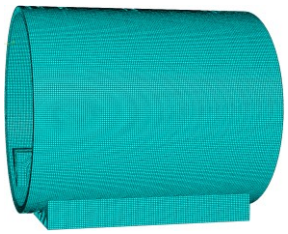

Figure 8. Finite element model under a rigid base.

Under this installation condition, the first six natural frequencies of the structure are listed in **Table 3**, and the corresponding mode shapes are shown in **Figure 9**. Compared with the free state (**Figure 7**), it is evident that the change in installation stiffness has led to significant variations in the structural modes.

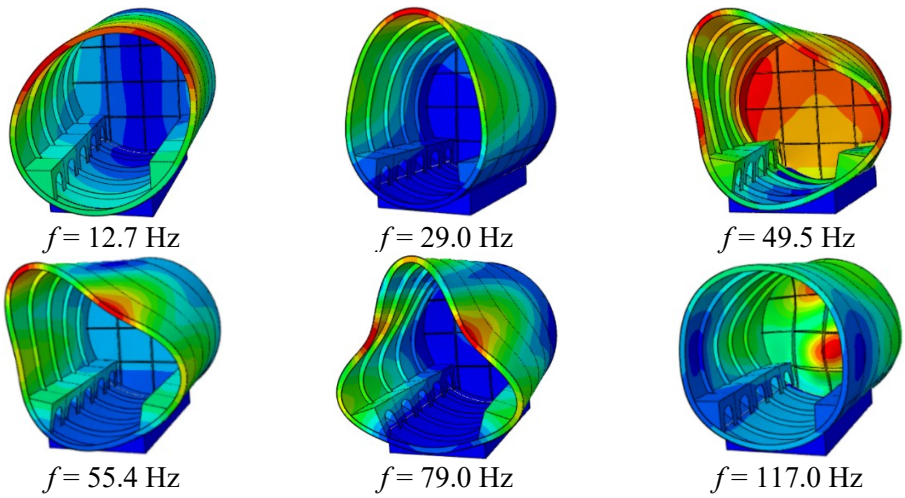

Figure 9. Mode shape cloud diagram under a rigid base.

Table 3. Natural frequency under a rigid base.

Mode order	1 (Hz)	2 (Hz)	3 (Hz)	4 (Hz)	5 (Hz)	6 (Hz)
Rigid base	12.7	29.0	49.5	55.4	79.0	117.0

4.3. Modal analysis under a rubber pad-supported base

Figure 10 presents the finite element model of the structure under rubber pad installation conditions.

Figure 10. Finite element model under a rubber pad-supported base.

Through modal analysis, the first six natural frequencies of the structure under rubber pad installation are obtained, as listed in **Table 4**. The corresponding mode shapes are shown in **Figure 11**, exhibiting relatively uniform deformation patterns.

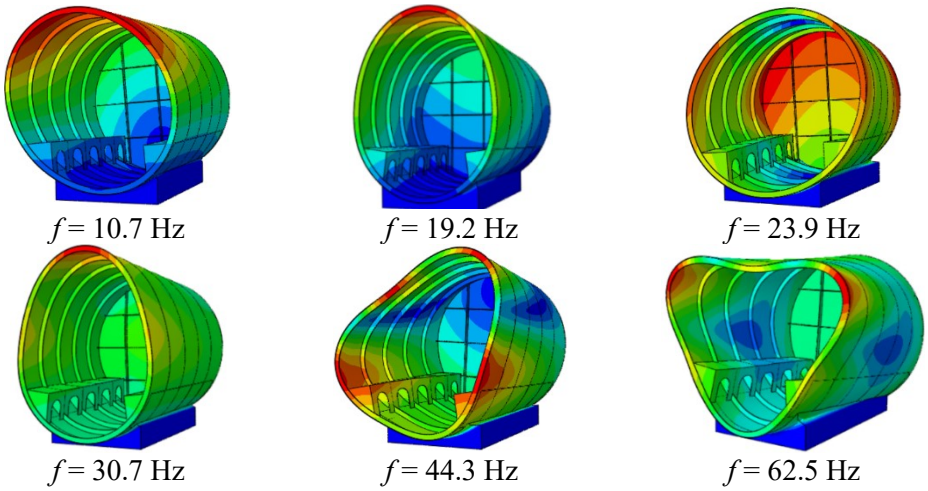

Figure 11. Mode shape cloud diagram under a rubber pad-supported base.

Table 4. Natural frequency under a rubber pad-supported base.

Mode order	1 (Hz)	2 (Hz)	3 (Hz)	4 (Hz)	5 (Hz)	6 (Hz)
Rubber pad-supported base	10.7	19.2	23.9	30.7	44.3	62.5

4.4. Modal analysis under a vibration isolator-supported base

Figure 12 illustrates the finite element model of the structure under vibration isolator-supported conditions, which is used to analyze the vibration characteristics in this installation state.

Figure 12. Finite element model under a vibration isolator-supported base.

The first six natural frequencies in this condition are listed in **Table 5**, and the corresponding mode shapes are shown in **Figure 13**. Compared with other installation conditions, the vibration characteristics under this state are closer to those of the free state shown in **Figure 7**.

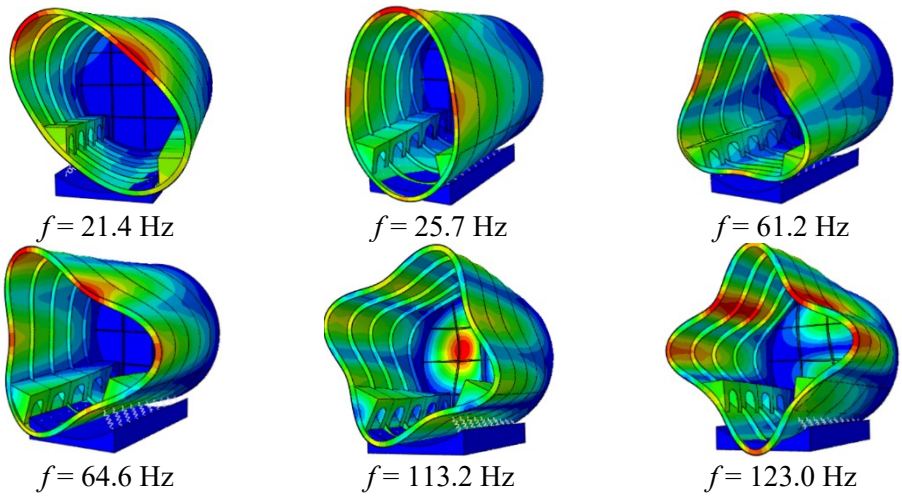

Figure 13. Mode shape cloud diagram under a vibration isolator-supported base.

Table 5. Natural frequency under a vibration isolator-supported base.

Mode order	1 (Hz)	2 (Hz)	3 (Hz)	4 (Hz)	5 (Hz)	6 (Hz)
Vibration isolator-supported base	21.4	25.7	61.2	64.6	113.2	123.0

4.5. Modal comparison analysis

Taking the same mode shape as an example, the changes in natural frequency under different installation stiffness conditions were compared, as detailed in **Table 6**.

Table 6. Comparison of natural characteristics under different installation stiffness conditions.

Free state	Rigid base	Rubber pad-supported base	Vibration isolator-supported base
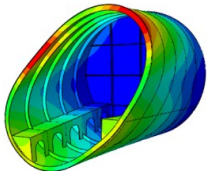	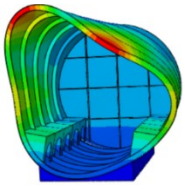	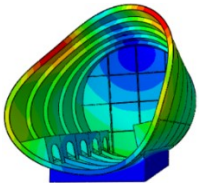	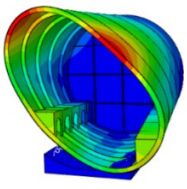
f = 22.1 Hz	f = 55.4 Hz	f = 36.7 Hz	f = 21.4 Hz

Table 6. (*Continued*).

Free state	Rigid base	Rubber pad-supported base	Vibration isolator-supported base
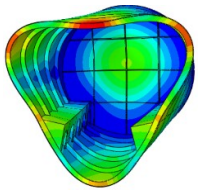	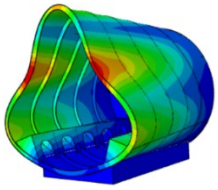	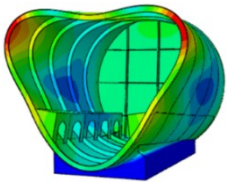	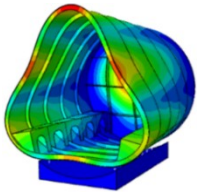
f = 62.8 Hz	f = 79.0 Hz	f = 62.5 Hz	f = 61.2 Hz
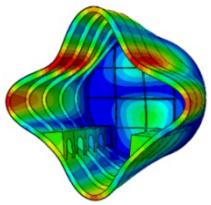	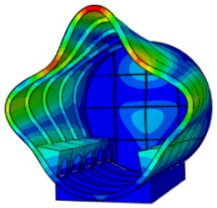	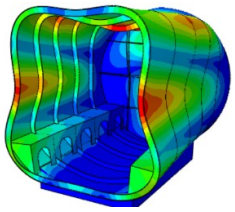	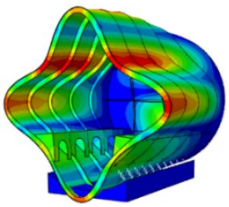
f = 124.9 Hz	f = 147.5 Hz	f = 123.7 Hz	f = 122.9 Hz

For ease of comparison (**Table 7**), the relative change Δf_i is defined as follows:

$$\Delta f_i(\%) = \frac{f_{i,\text{base}} - f_{i,\text{free}}}{f_{i,\text{free}}} \times 100\% \tag{15}$$

where $f_{i,\text{base}}$ is the natural frequency of the i-th mode under the installed base condition, and $f_{i,\text{free}}$ is the natural frequency in the free state.

Table 7. Analysis of the influence of installation stiffness on the natural frequency of the structure.

Mode (Hz)	1st mode	Δf_i(%)	2nd mode	Δf_i(%)	3rd mode	Δf_i(%)
Free state	22.1		62.8		124.9	
Rigid base	55.4	**150.679**	79.0	**25.796**	147.5	**18.094**
Rubber pad-supported base	36.7	**66.063**	62.5	**0.478**	123.7	**0.961**
Vibration isolator-supported base	21.4	**3.167**	61.2	**2.548**	122.9	**1.601**

4.6. Results analysis

Through modal analysis of the shell under different installation stiffness base conditions, three cases were considered: rigid base, rubber pad-supported base, and vibration isolator-supported base. The natural frequencies of the stiffened cylindrical shell were calculated under a range of installation stiffness conditions and compared with the natural frequencies in the free state [29]. The results indicate that different installation stiffness has a significant impact on the natural frequencies and vibration characteristics of the stiffened cylindrical shell.

4.6.1. The impact of installation stiffness on vibration characteristics

From the mode shape analysis, it can be observed that under the rigid base condition, the free deformation of the stiffened cylindrical shell is significantly restricted, especially the bottom displacement, which is strongly constrained. The mode shape mainly exhibits localized deformation, with the deformation concentrated at the open end of the cylindrical shell. Under the rubber pad-supported base condition, the overall stiffness decreases, and the deformation at the bottom is more noticeable

compared to the rigid base. In the case of vibration isolator-supported installation, the deformation mode of the shell is freer compared to other installation stiffness conditions, with the structural deformation almost identical to the deformation mode in the free state.

4.6.2. Comparison of natural frequencies under the same mode shape

Through a detailed analysis of the natural frequencies and relative changes of the structure under different installation stiffness conditions presented in **Table 6**, this study found that the variation in natural frequencies primarily occurs in the lower-order modes. Based on Equation (14) $\Delta\omega_i \propto \sum_j \frac{(\phi_{i,j})^2}{2\omega_i}\Delta k_j$, under the rigid base condition, the natural frequency of mode 1 increases from 22.1 Hz to 55.4 Hz relative to the free-state structure, with a relative change exceeding 150%. This is consistent with the theoretical prediction $\frac{\partial\omega_i}{\partial k_j} \propto \frac{1}{2\omega_i}$. The 2nd and 3rd modes also show significant increases, but the amplitude of increase gradually decreases as the mode order rises. The finite element results show that as the installation stiffness increases, the natural frequency shifts to higher frequency ranges, significantly raising the natural frequencies of the cylindrical shell [30], with a particularly noticeable impact on the low-frequency modes.

Under the rubber pad-supported base condition, the relative change in the natural frequency of mode 1 is 66.06%. Although there is a noticeable deviation in mode 1, the frequency change for other modes is $\Delta f_i \leq 1\%$, which is significantly smaller than under the rigid base condition and is almost identical to the free state. This suggests that the rubber pad-supported base can effectively retain the original vibration characteristics at mid-to-high frequencies.

In the case of the vibration isolator-supported base, with isolators installed on both sides of the stiffened cylindrical shell, the natural frequencies are similar to those in the free state, closely matching the free vibration state of the stiffened cylindrical shell. This indicates that the vibration isolator-supported base retains the natural frequencies close to the free vibration state of the structure compared to other installation stiffness conditions.

4.6.3. Sensitivity verification based on theoretical formula

Based on the sensitivity relationship between natural frequency and installation stiffness in Equation (13):

$$\frac{\partial\omega_i}{\partial k_j} = \frac{1}{2\omega_i}\left(\phi_{i,j}\right)^2$$

it can be seen that the change in natural frequency $\Delta\omega_i$ is proportional to the square of the displacement component of the modal shape at the installation position $\left(\phi_{i,j}\right)^2$, and inversely proportional to the current order of the natural frequency ω_i (Equation (14)). For low-order modes (e.g., the 1st mode), their natural frequency ω_i is relatively small, so the attenuation effect of the denominator term $2\omega_i$ is weak. Moreover, the overall displacement amplitude of the low-order mode at the support position, $\phi_{i,j}$, is generally larger (as seen in the overall bending mode in the free state shown in **Figure 7**). Therefore, the same change in stiffness Δk_j has a more significant impact on low-

order frequencies. In contrast, for high-order modes, ω_i is higher, and the mode shape becomes more localized (e.g., localized buckling of the shell). The displacement component at the support position, $\phi_{i,j}$ is smaller, which leads to a reduced sensitivity to stiffness changes.

5. The impact of rubber pad parameters on natural frequency

From the analysis of the above results, it can be concluded that under the rigid base condition, the natural frequency of the structure increases significantly, demonstrating a strong rigidity effect. In contrast, the vibration isolator-supported base can effectively approach the ideal vibration isolation state, achieving better vibration isolation performance. The rubber pad-supported base shows a noticeable difference only in the first-order natural frequency, but for other frequencies, it closely resembles the ideal state. Based on this, the impact of key parameters such as rubber pad thickness and elasticity modulus on the natural characteristics of the stiffened cylindrical shell was further explored. Compared to the other two installation methods, the rational selection and use of an appropriate rubber pad not only meets the diverse vibration isolation needs but also enables quick adjustment and optimization of the installation method. This, in turn, provides more targeted solutions for vibration isolation design.

5.1. The influence mechanism of rubber pad materials

The thickness and elastic modulus of rubber are key parameters in evaluating the performance of rubber pads [31]. Increasing the rubber thickness generally makes the material softer in vibration isolation applications. Additionally, a high elastic modulus indicates that the material has a more crystalline structure, making it stiffer. In contrast, a low elastic modulus suggests that the material has a more amorphous structure, making it more flexible [32].

The stiffness of the rubber pad-supported base mainly depends on the stiffness of the rubber material [33]. According to elastic mechanics theory, under uniform compression conditions, the stiffness k of the rubber pad can be calculated using Equation (16):

$$k = \frac{E \times A}{h} \tag{16}$$

where A is the contact area of the rubber pad, h is the total thickness of the rubber layer, and E is the elastic modulus of the rubber.

In the vibration analysis of elastic support structures, the basic description is the single degree of freedom (SDOF) vibration system, whose natural frequency expression is:

$$\omega_n = \sqrt{\frac{k}{m}} \tag{17}$$

where ω_n is the system's natural angular frequency, k is the system's equivalent stiffness, and m is the system's equivalent mass.

Substituting this into the natural frequency equation, we get:

$$\omega_n = \sqrt{\frac{EA}{mh}} \tag{18}$$

The conclusion that can be drawn from this is that increasing the rubber thickness h or decreasing the elastic modulus E of the rubber will result in a reduction of the system's stiffness k, thereby decreasing the natural frequency ω_n.

In classical vibration isolation theory, to improve the isolation effect, the system's natural frequency should be as low as possible compared to the excitation frequency ω_{exc}. This is typically defined by the isolation frequency ratio:

$$\Upsilon = \frac{\omega_{exc}}{\omega_n} \tag{19}$$

According to theory, when the isolation frequency ratio Y > $\sqrt{2}$ the vibration isolation effect is significant. A common engineering approach to reduce the natural frequency ω_n is by increasing the thickness of the rubber layer or using materials with a lower elastic modulus.

5.2. The effect of rubber pad thickness on the structural natural frequency

The initial rubber pad used in this study had a thickness of 50 mm. Since the common thickness range for rubber pads in the market is 10–100 mm, with 10–100 mm being the standard specifications available for direct purchase, it is necessary to ensure that the selected parameters not only meet the procurement availability from the supply chain but also achieve the required functionality. Based on this, as displayed in **Table 8**, the effects of rubber pad thicknesses of 70 mm, 60 mm, 40 mm, and 30 mm on the inherent characteristics of the reinforced cylindrical shell were further investigated [34].

Table 8. Comparison of the natural characteristics of the structure under different rubber pad thicknesses.

70 mm	60 mm	50 mm	40 mm	30 mm
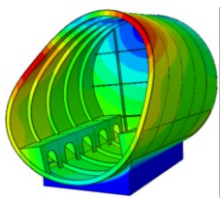	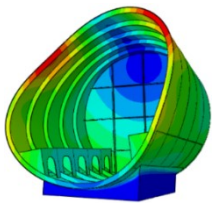	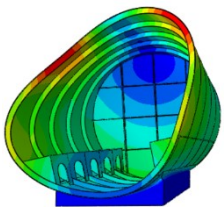	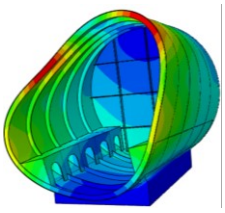	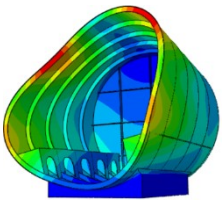
f = 32.7 Hz	f = 34.3 Hz	f = 36.7 Hz	f = 38.1 Hz	f = 40.2 Hz
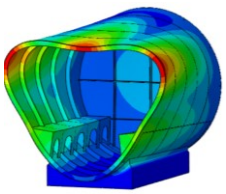	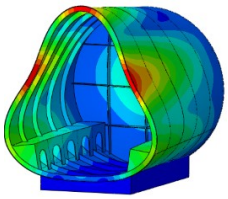	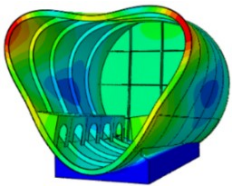	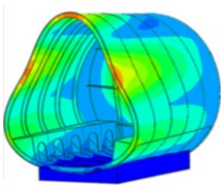	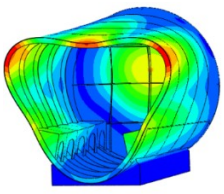
f = 59.9 Hz	f = 59.3 Hz	f = 62.5 Hz	f = 61.8 Hz	f = 63.2 Hz

Table 8. (*Continued*).

70 mm	60 mm	50 mm	40 mm	30 mm
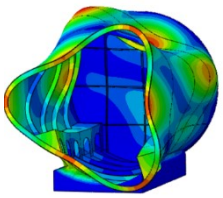	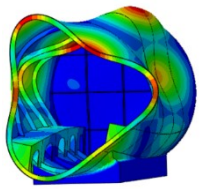	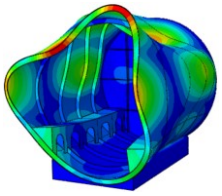	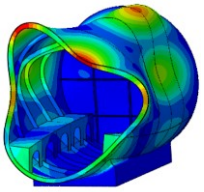	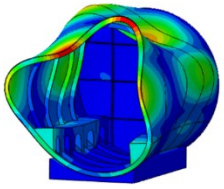
f = 133.1 Hz	f = 132.0 Hz	f = 133.4 Hz	f = 134.1 Hz	f = 135.2 Hz

5.3. The effect of the rubber pad's elastic modulus on the structural natural frequency

To further investigate the impact of rubber material hardness on the system's vibration characteristics, this study selected a 60 mm thick rubber pad as the reference and analyzed the changes in the natural characteristics of the stiffened cylindrical shell when the elastic modulus was 5 MPa, 4 MPa, 3 MPa, and 2 MPa, as shown in **Table 9**.

Table 9. Comparison of structural natural characteristics under rubber pads with different elastic moduli.

5 MPa	4 MPa	3 MPa	2 MPa
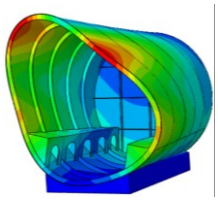	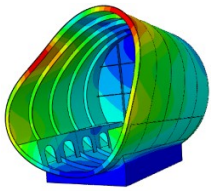	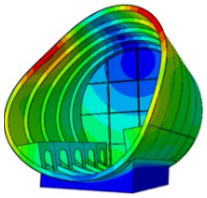	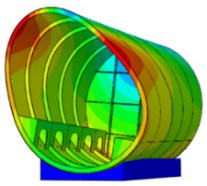
f = 38.5 Hz	f = 37.0 Hz	f = 34.3 Hz	f = 49.4 Hz
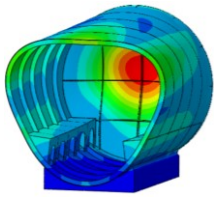	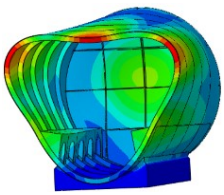	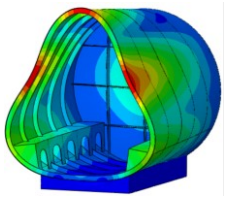	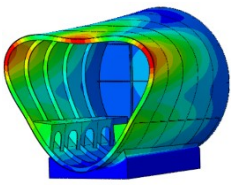
f = 61.8 Hz	f = 60.7 Hz	f = 59.3 Hz	f = 57.1 Hz
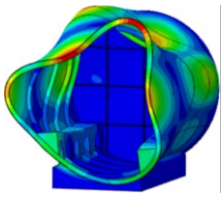	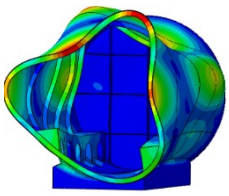	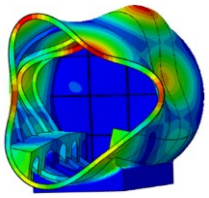	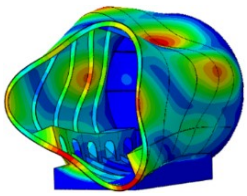
f = 124.9 Hz	f = 147.5 Hz	f = 123.7 Hz	f = 122.9 Hz

5.4. Result analysis

In the experiment, the effects of rubber pad thickness and elastic modulus on the natural frequencies and vibration modes of the stiffened cylindrical shell were analyzed. The results in **Figure 14** and **Table 10** show that the rubber pad thickness has varying sensitivity to the natural frequencies and vibration modes at different

modes. In the low-order natural frequency range, the variation of rubber pad thickness significantly affects both the natural frequency and vibration mode; however, at higher-order natural frequencies, the effect is relatively smaller. This phenomenon can be attributed to the fact that low-order natural frequencies primarily reflect the overall vibration characteristics of the structure, and the variation in rubber pad thickness has a more significant impact on the overall stiffness and boundary conditions of the structure, leading to a more noticeable effect on low-order natural frequencies and modes. On the other hand, high-order natural frequencies reflect more localized vibration characteristics, and the change in rubber pad thickness has a lesser effect on local vibrations.

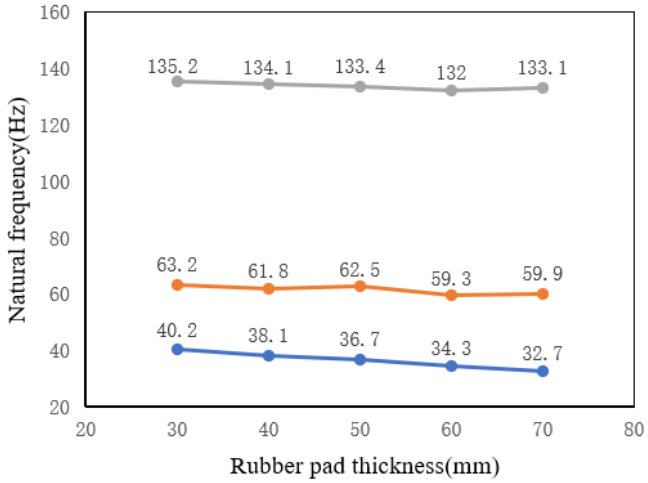

Figure 14. The effect of rubber pad thickness on the structural natural frequency curve.

Table 10. Analysis of the impact of rubber pad thickness on the structural vibration characteristics.

	Mode (Hz)					
Rubber pad thickness	**1st mode**	**Δf_i (%)**	**2nd mode**	**Δf_i (%)**	**3rd mode**	**Δf_i (%)**
Free state	**22.1**		**62.8**		**129.9**	
70 mm	32.7	**47.964**	59.9	**−4.618**	133.1	**2.463**
60 mm	34.3	**55.204**	59.3	**−5.573**	132.0	**1.617**
50 mm	36.7	**66.06**	62.5	**−0.48**	133.4	**2.69**
40 mm	38.1	**72.398**	61.8	**−1.592**	134.1	**3.233**
30 mm	40.2	**81.900**	63.2	**0.637**	135.2	**4.080**

Through systematic analysis of **Figure 15** and **Table 11**, we demonstrate that a decrease in the elastic modulus of the rubber pad leads to a clear downward trend in the natural frequencies of the stiffened cylindrical shell. For example, in the first mode, when the elastic modulus decreases from 5 MPa to 2 MPa, the first natural frequency decreases from 38.5 Hz to 29.4 Hz, a reduction of approximately 23.64%. From the perspective of material mechanics, the elastic modulus E is positively correlated with stiffness, i.e., $k \propto E$. When the elastic modulus is lower, the stiffness of the rubber pad is smaller, resulting in weaker constraint on the reinforced cylindrical shell, which

increases the freedom of vibration and makes deformation more likely, thereby further reducing the natural frequency.

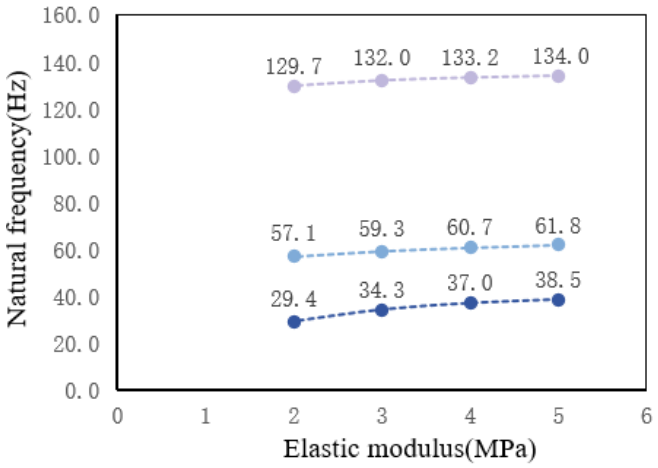

Figure 15. The effect of rubber pad elastic modulus on the structural natural frequency curve.

Table 11. The impact of rubber pads with different elastic moduli on structural vibration characteristics.

	Mode (Hz)					
Elastic modulus of rubber pad	**1st mode**	**Δf_i (%)**	**2nd mode**	**Δf_i (%)**	**3rd mode**	**Δf_i (%)**
Free state	**22.1**		**62.8**		**129.9**	
5 MPa	38.5	**74.208**	61.8	**−1.592**	134.0	**3.156**
4 MPa	37.2	**68.326**	60.7	**−3.344**	133.2	**2.540**
3 MPa	34.3	**55.20**	59.3	**−5.57**	132.0	**1.62**
2 MPa	29.4	**33.032**	57.1	**−9.076**	129.7	**−0.154**

In engineering practice, the selection of rubber pads should consider the vibration characteristics of the reinforced cylindrical shell, the installation environment, and the vibration isolation requirements. In situations where a higher vibration isolation effect is needed, softer and thicker rubber pads can effectively lower the natural frequencies and optimize the vibration isolation performance. However, it should be noted that excessively thick or soft rubber pads may reduce the support stiffness and affect the structural stability. Therefore, it is also important to properly adjust the rubber pad parameters to achieve the best installation effect during the design process.

6. Conclusions

To more accurately simulate the dynamic characteristics of an underwater vehicle in its actual working state, the installation stiffness and support method should closely approximate the natural characteristics in the free state. This study focuses on a stiffened cylindrical shell structure, employing finite element simulation analysis to systematically investigate the influence of installation stiffness on the natural characteristics of the stiffened cylindrical shell and analyze the effect of rubber pad parameters on the structural vibration characteristics. The main conclusions are as follows:

(1) The study shows that the natural frequency and vibration modes of the structure are significantly affected by installation stiffness. Based on the equation $\Delta\omega_i \propto \sum_j \frac{(\phi_{i,j})^2}{2\omega_i}\Delta k_j$ and simulation data analysis, it is observed that as installation stiffness increases, the natural frequency also increases, especially for lower-order modes. Under high installation stiffness conditions, the degrees of freedom for vibration are constrained, shortening the vibration path and thereby increasing the natural frequency. In contrast, under low stiffness conditions, the natural frequency decreases significantly. Furthermore, higher installation stiffness results in stronger boundary constraints, limiting the free deformation of the shell, particularly at the bottom, leading to localized deformation, with the deformation area concentrated at the open end of the cylindrical shell. Under low stiffness conditions, bottom deformation is more noticeable, and the vibration mode approaches the free state.

(2) In frequency bands above 50 Hz, the natural frequency of the rubber pad-supported base remains consistent with that in the free state, effectively preserving the structural vibration characteristics. Experimental analysis indicates that the thickness and elastic modulus of the rubber pad significantly influence lower-order natural frequencies. Specifically, increasing the thickness or reducing the elastic modulus decreases the system stiffness, thereby lowering the natural frequency. While proper selection of rubber pad parameters can reduce the structural natural frequency to some extent, it is critical to note that rubber pads may undergo permanent deformation under high static or impact loads. Prolonged static loading can also induce creep effects, and their stiffness and damping properties vary significantly with temperature. To ensure long-term reliability in engineering applications, the vibration isolation system should integrate load verification, creep testing, and temperature adaptability evaluations. Additionally, appropriate safety factors must be applied to balance vibration isolation performance with structural stability under diverse operational conditions.

(3) This study, consistent with references [12], finds that lower-order natural frequencies are highly sensitive to changes in boundary stiffness. For example, under rigid base conditions, the first-order frequency of the reinforced cylindrical shell with an added rubber pad increases by 150.68%. In reference [12], experimental validation showed that stiffness adjustment could shift the resonance frequency by up to 20%. Through both experiments and numerical simulations, the study investigated the influence of edge stiffness on the vibration characteristics of an open square box structure [35], revealing that a 20% increase in edge stiffness could raise the fundamental frequency by 18%, but also intensifies mode coupling. This indicates that the sensitivity of low-order modes to stiffness variations exhibits cross-structural universality.

Author contributions: Conceptualization, LL and JG; methodology, LL; software, LL; validation, LL, JG and JX; formal analysis, LL; investigation, JX; resources, HL; data curation, LL; writing—original draft preparation, LL; writing—review and editing, CG; visualization, LL; supervision, HL; project administration, HL; funding acquisition, FP. All authors have read and agreed to the published version of the manuscript.

Funding: This study was funded by National Natural Science Foundation of China (52371314), Fundamental Research Funds for the Central Universities (3072024XX0102, 3072024JJ0101), and Natural Science Foundation of Heilongjiang Province (YQ2023E035).

Institutional review board statement: Not applicable.

Informed consent statement: Not applicable.

Conflict of interest: The authors declare no conflict of interest.

References

1. Wu JH, Sun YD, Duan Y. Exact solutions for free and forced vibrations of cross-ply composite laminated combined conical–cylindrical shells with arbitrary boundary conditions. Ocean Engineering. 2023; 285(P1).
2. Bai X, Xu W, Ren H, et al. Analysis of the influence of stiffness reduction on the load carrying capacity of ring-stiffened cylindrical shell. Ocean Engineering. 2017; 135: 52–62.
3. Qin Z, Chu F, Zu J. Free vibrations of cylindrical shells with arbitrary boundary conditions: A comparison study. International Journal of Mechanical Sciences. 2017; 133: 91–99.
4. Luo X, Zhou H, Li L, et al. Acoustic vibrations of underwater double-walled cylindrical shells with elastically restrained boundaries. Applied Ocean Research. 2025; 154: 104426.
5. Zhang CY, Jin GY, Wang ZH, Sun Y. Dynamic stiffness formulation and vibration analysis of coupled conical-ribbed cylindrical-conical shell structure with general boundary condition. Ocean Engineering. 2021; 234: 109294.
6. Pang F, Tang Y, Li C, et al. Reconstructed source method for underwater noise prediction of a stiffened cylindrical shell. Ocean Engineering. 2024; 310(P2): 118828.
7. Du Y, Sun L, Li S, Li Y. Vibration analysis of truncated spherical shells under various edge constraints. Thin-Walled Structures. 2020; 147: 106544.
8. Liu C, Wang Y, Zhang W, et al. Nonlinear dynamics of a magnetic vibration isolator with higher-order stable quasi-zero-stiffness. Mechanical Systems and Signal Processing. 2024; 218: 111584.
9. Li H, Xu J, Pang F, et al. A unified Jacobi-Ritz-spectral BEM for vibro-acoustic behavior of spherical shell. Computers and Mathematics with Applications. 2024; 176: 415–431.
10. Liu C, Zhang W, Yu K, et al. Quasi-zero-stiffness vibration isolation: Designs, improvements and applications. Engineering Structures. 2024; 301: 117282.
11. Liu C, Zhao R, Yu K, et al. A quasi-zero-stiffness device capable of vibration isolation and energy harvesting using piezoelectric buckled beams. Energy. 2021; 233.
12. Xu Z, Tang D, Xu D, et al. The influence mechanism of transmission stiffness on mechanical resonance of aircraft rudder servo system. Journal of Physics: Conference Series. 2025; 2955(1): 012015.
13. Wang Z, Wang Y, Xu Z, et al. Modeling and Free Vibration Analysis of Dual-Functionally Graded Carbon Nanotube Reinforced Composite Stepped Cylindrical Shells with Arbitrary Boundary Conditions. Mechanics of Solids. 2024; 59(4): 2594–2616.
14. Sobhani E, Masoodi RA, Ahmadi-Pari AR. Circumferential vibration analysis of nano-porous-sandwich assembled spherical-cylindrical-conical shells under elastic boundary conditions. Engineering Structures. 2022; 273.
15. Hua L. Frequency analysis of rotating truncated circular orthotropic conical shells with different boundary conditions. Composites Science & Technology. 2000; 60(16): 2945–2955.
16. Pang F, Tang Y, Qin Y, et al. Analysis of acoustic radiation characteristic of laminated paraboloidal shell based on Jacobi-Ritz-spectral BEM. Ocean Engineering. 2023; 280.
17. Li HJ, Taniguchi Y. Effect of joint stiffness and size on stability of three-way single-layer cylindrical reticular shell. International Journal of Space Structures. 2020; 35(3): 90–107.
18. Gao C, Pang F, Li H, Wang X. Forced Vibration Analysis of Uniform and Stepped Circular Cylindrical Shells with General Boundary Conditions. International Journal of Structural Stability and Dynamics, 2022, 22(12).
19. Zheng D. Vibration characteristic analysis of thin-walled conical shells with arbitrary thickness variation and general boundary condition. Thin-Walled Structures. 2025; 212: 113160.

20. Yang F, Zhang Y, Li H. Vibration analysis of rotating rings with complex support stiffnesses. MATEC Web of Conferences. 2018; 237.
21. Zhang C, Yi X, Ma W, et al. Study on the influence of structural form and parameters on vibration characteristics of typical ship structures. Reviews on Advanced Materials Science. 2022; 61(1): 16–26.
22. Bashir S, Mandhaniya P, Akhtar N. Influence of Vibration Isolator Stiffness on the Dynamic Performance of a Steel-Floating Slab Track. In: Proceedings of the 15th International Conference on Vibration Problems; 14–17 November 2021; Doha, Qatar.
23. Chen T, Trogdon T. Stability of the Lanczos algorithm on matrices with regular spectral distributions. Linear Algebra and its Applications. 2024; 682: 191–237.
24. Peng G, Gong X, Wang S, et al. Sparse Regularization Least-Squares Reverse Time Migration Based on the Krylov Subspace Method. Remote Sensing. 2025; 17(5): 847–847.
25. Ministry of Housing and Urban-Rural Development of the People's Republic of China. Code for Design of Building Vibration Isolation: GB 50463–2019. China Planning Press; 2019.
26. Liu Zhe, Wang W, Wu S, et al. Model Design and Experimental Study of Cabin Raft Isolation System with Space Truss Structure (Chinese). China Shipbuilding. 2024; 65(6): 10–21.
27. Li H, Xu J, Gong Q, et al. A study on the dynamic characteristics of the stiffened coupled plate with the effect of the dynamic vibration absorbers. Computers and Mathematics with Applications. 2024; 168: 120–132.
28. Kolarevi N, Nefovska-Danilovi M. Dynamic stiffness—based free vibration study of open circular cylindrical shells. Journal of Sound Vibration. 2020; 486.
29. Liu JY. Gu YS, Yang ZC. Influence of support stiffness on natural mode and body freedom flutter characteristics of flying wing model (Chinese). Journal of Vibration Engineering. 2018; 31(5): 727–733.
30. Fu T, Wu X, Xiao Z, et al. Analysis of vibration characteristics of FGM sandwich joined conical–conical shells surrounded by elastic foundations. Thin-Walled Structures. 2021; 165.
31. Costa Vieira J, Mendes AdO, Leite Ribeiro M, et al. FEM Analysis Validation of Rubber Hardness Impact on Mechanical and Softness Properties of Embossed Industrial Base Tissue Papers. Polymers. 2022; 14(12): 2485.
32. Schaefer RJ. Chapter 33—Mechanical Properties of Rubber. In: Harris' Shock and Vibration Handbook. The McGraw-Hill; 2009.
33. Yang Y, Li T, Dai K, et al. Vertical stiffness reduction of rubber bearings under lateral displacement considering different shape factors. Construction and Building Materials. 2024; 426.
34. Wang J, Du B. Experiment on the optimization of sound insulation performance of residential floor structure. Applied Acoustics. 2020; 174: 107734.
35. Chiba M, Hiraoka S, Nakase A. Effect of Edge Stiffness on Vibration Characteristics of Upper-Opening Square-Base Box-Type Structures. Journal of Vibration Engineering & Technologies. 2024; 12(Suppl 2): 1849–1873.